Improved efficiency of organic solar cells using Au NPs incorporated into PEDOT:PSS buffer layer

Francis Otieno,[1,3,5,a] Ndivhuwo P. Shumbula,[2] Mildred Airo,[2] Mlambo Mbuso,[4] Nosipho Moloto,[2,3] Rudolph M. Erasmus,[1,3] Alexander Quandt,[1,3,5] and Daniel Wamwangi[1,3,5]

[1]*Material Physics Research Institute, School of Physics, University of the Witwatersrand, Private Bag 3, Wits 2050, Johannesburg, South Africa*
[2]*School of Chemistry, University of the Witwatersrand, Private Bag 3, Wits 2050, Republic of South Africa*
[3]*Materials for Energy Research group, University of the Witwatersrand, Private Bag 3, 2050 Wits, Johannesburg, South Africa*
[4]*Department of Physics, University of Pretoria, Pretoria 0002, South Africa*
[5]*Museo Storico della Fisica e Centro Studi e Ricerche Enrico Fermi, Piazza del Viminale 1, 00184 Roma, Italy*

(Received 24 April 2017; accepted 27 July 2017; published online 4 August 2017)

Au based plasmonic phenomenon inside the hole transport layer poly(3,4-ethylenedioxythiophene)-poly(styrenesulfonate) (PEDOT:PSS) of an organic solar cell based on blend of poly(3-hexylthiophene) (P3HT) and [6:6]-phenyl-C61-butyric acid (PCBM) is investigated. The concentration of the Au nanoparticles synthesized by wet chemical reduction is one of the key factors to strong light trapping when the spherical gold nanoparticles are blended into the PEDOT:PSS solution. Studies of the influence of the concentration of nanoparticles distribution in the PEDOT:PSS were carried out using UV–Vis spectroscopy and atomic force microscopy. Electrical characteristics of the pristine device and of device with metallic nanostructures were analyzed from J –V characteristics to observe the plasmonic effects on the performance in the P3HT:PCBM organic solar cells. The origin of the photocurrent enhancements with varying Au nanoparticles concentrations on PEDOT:PSS are discussed. [http://dx.doi.org/10.1063/1.4995803]

I. INTRODUCTION

Organic solar cells (OSCs) based on conducting polymers and small molecular weight organic semiconductors have attracted much research interest.[1,2] This is because they are likely to be a promising renewable technology for the collection and conversion of solar energy using devices fabricated out of solutions active materials. These materials thus employ inexpensive, scalable printing techniques that has less environmental impact.[3,4] However, the mass production of OSCs for commercialization is hindered by low efficiency as well as lifetime instability[5] hence the need for the further performance enhancement to enable them become a low-cost alternative to the commonly available conventional inorganic solar cells.

A very promising approach for the fabrication of OSCs is based on the concept of bulk-heterojunction (BHJ), a 3D network of nano-separated domains of P3HT[6] as an electron donor and {[6,6]-phenyl C61 butyric acid methyl ester} as an electron acceptor. The interconnectivity of the network provides an increased interfacial contact area between the donor and acceptor within the dimensions of the exciton diffusion length. This enhances the ability for excitons to diffuse to the donor-acceptor interface and separate before recombination.[7] However, BHJ network also suffer from

[a]Corresponding Author: Francis Otieno Email: frankotienoo@gmail.com

short exciton diffusion lengths (10–20 nm)[8] as well as poor charge mobility (10^{-5} to 10^{0} cm^2/V s) as a result of the low refractive index of the conjugated polymers which adversely leads to an increase in the germinate recombination probability.[9] The short diffusion length limits the thickness of the active layer to 100–200 nm leading to low light absorption.[10] Light management schemes can be used to increase the dwell time and light interaction in the active layer. Among the many approaches to absorption enhancement, light trapping by geometrical nanostructures is extensively investigated. Light trapping can be improved through the use of plasmonically active nanoparticles producing a localized surface plasmon resonance (LSPR).

A surface plasmon wave is optically generated and propagates along the metal/dielectric interface. A resonance can be achieved while tuning the excitation light when the frequency of the incident photons is equal to the collective oscillation frequency of the free electrons of metallic nano-particles.[11] This resonance usually strongly depends on the nanoparticle size, shape, and distribution as well as on the metal's dielectric functions together with its dielectric surrounding environment.[12]

Several groups have reported the applications of metallic noble nanostructures geared towards enhancing the performance solar cell of devices[8,13–15] by an introduction of metal nanoparticles into active layer (P3HT:PCBM blend),[16] poly (3,4-ethylene dioxythiophene:poly (styrenesulfonate) (PEDOT:PSS) used as hole transport layer,[17,18] or both of the two.[19]

In the present work, comparative results on the OSCs performance with varied volume ratio of Au NPs in the PEDOT:PSS matrix are presented. The Au NPs of diameter 11±3 nm were synthesized using chemical reduction method. The absorption enhancement in the active layer despite the dispersal of the Au NPs in PEDOT:PSS is attributed to LSPR by broad band scattering which produce a lateral field along the layer.[20] An increase in short-circuit current density (J_{SC}), corresponding to the enhancement of power conversion efficiency (PCE), by about 48.2 % for the Au Np incorporated device is demonstrated.

II. EXPERIMENTAL DETAILS

A. Synthesis of Au NPs

Au NPs were synthesized using chemical reduction procedure in which an aqueous solution of 1mM $HAuCl_4$, 100ml was first heated to boil. To the boiling solution, 40 ml of an aqueous solution of 0.04mM Tri-sodium citrate was added while stirring. The mixture was further heated until the ruby red colour appeared (after 7 minutes), indicating the formation of gold nanoparticles. Then the mixture was removed from the heat and stirred continuously for further 3 hours in water solution. The citrate ions also as acted as stabilizer.

B. Device fabrication and characterization

Different Au NPs concentrations in PEDOT:PSS layers were prepared by adding 1, 2, 4, 6 and 8 ml of Au NPs solution into 100 ml of PEDOT:PSS (1.3 wt% dispersion in H_2O) to form different volume ratio (ratio of Au-NPs solution to PEDOT:PSS solution). The resulting solutions were ultra-sonicated for 30 minutes before being spin-coated onto ITO-coated glass substrates. The ITO substrate were pre-cleaned and dried in procedure described elsewhere.[8] PEDOT:PSS and a blend of Au and PEDOT:PSS was then spin-coated on top of the ITO layer at a speed of 2000 rpm for 60 seconds and then annealed over a hot plate at 100 °C for 10 min to remove any residual water. The resulting thickness of PEDOT:PSS was measured by a surface profilometer to 30 nm. The active layer comprising P3HT:PCBM polymer blend solution (Sigma-Aldrich) was prepared by mixing P3HT and PCBM at 1 : 1 ratio in chlorobenzene, with a total concentration of 20 mg/ml. The mixed solution was spin-coated at 2000 rpm for 60 seconds to form a homogenous film of thickness 215 nm. Aluminum cathode was then metalized through thermal evaporation. The complete device was then annealed in Argon ambient at 100 °C for 15 minutes to remove organic polymer solvent and any water residual. The thickness of the active layer is 220 nm. More than 50 devices each of area varying from 7.0 mm^2 to 8.5 mm^2 were fabricated, characterized and the results obtained showed a high degree of repeatability.

The morphologies and structural analyses of the samples were characterized using Veeco Di-3100 atomic force microscopy (AFM) in tapping mode and FEI Nova Nanolab 600 SEM. The elemental composition of the films were analysed through an energy dispersive X-ray spectrometer (EDX) attached to the SEM. The Raman bands and the structural order of all the films were examined using a Jobin Yvon T64000 Raman spectrometer equipped with an Ar ion laser (514.5 nm) and a laser power of 5 mW. The current density–voltage (J–V) characteristics were obtained using the solar simulator (150 W Xe lamp) with 1.5 air mass filters and a source/Measure unit (HP 4141B DC) unit under 100 mW/cm^2 illumination. All the measurements were carried out at room temperature under standard conditions.

III. RESULTS AND DISCUSSION

A. Morphology studies

1. Transmission electron microscopy (TEM)

Figure 1 shows the (TEM) image of gold nanoparticles and their size distribution in uniformly dispersed suspensions.

Au NPs were successfully synthesized using trisodium citrate as both reducing and capping moiety. Boiling the solution of $HAuCl_4$ at 97 °C in the presence of trisodium citrate resulted in the formation of Au NPs. This was indicated by the change from a colorless to deep ruby-red solution. The synthesized nanoparticles are monodispersed as deduced from TEM analysis. The analysis of about 200 Au nanoparticles from TEM images lead to Au NP size distribution as shown in Figure 1 b. According to the transmission electron microscopy (TEM) images and size distribution, the diameter of Au nanoparticles is was found to be 11 ± 0 .2 nm. Based on Beer's Lambert law the concentration of Au NPs in water was approximated to be 22 ± 3 mol/L.

2. Atomic force microscopy (AFM)

The surface morphology of the pristine PEDOT:PSS and for Au NP dispersed films were characterized using Veeco Di3100 AFM under tapping mode (Fig. 2).

The spherical Au NPs with an average diameter of about 11 ± 2 nm, are dispersed uniformly on the PEDOT:PSS below threshold percentage volume of 6%, beyond which particle agglomeration emerges. The Au NPs dispersion was easily distributed in the PEDOT:PSS dispersion as they both have a continuous phase of water.

The pristine PEDOT:PSS layer showed a relatively smooth surface with roughness (R_{rms}) of 4.3 nm. This roughness increases with an increase in nanoparticles concentration in the PEDOT:PSS. Table I shows a summary of surface topographic parameters; average roughness (R_a), Root mean square roughness (R_{rms}) and skewness (R_{sk}).

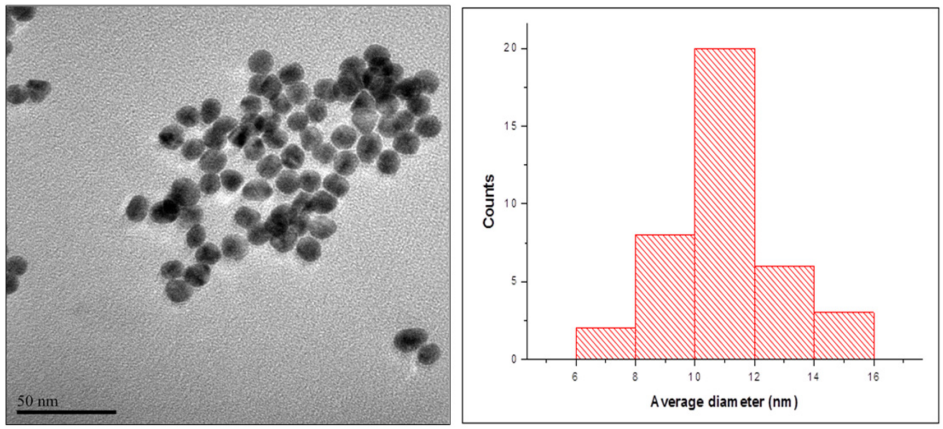

(a) (b)

FIG. 1. TEM Images of colloidal gold solution and bar graph of size distribution.

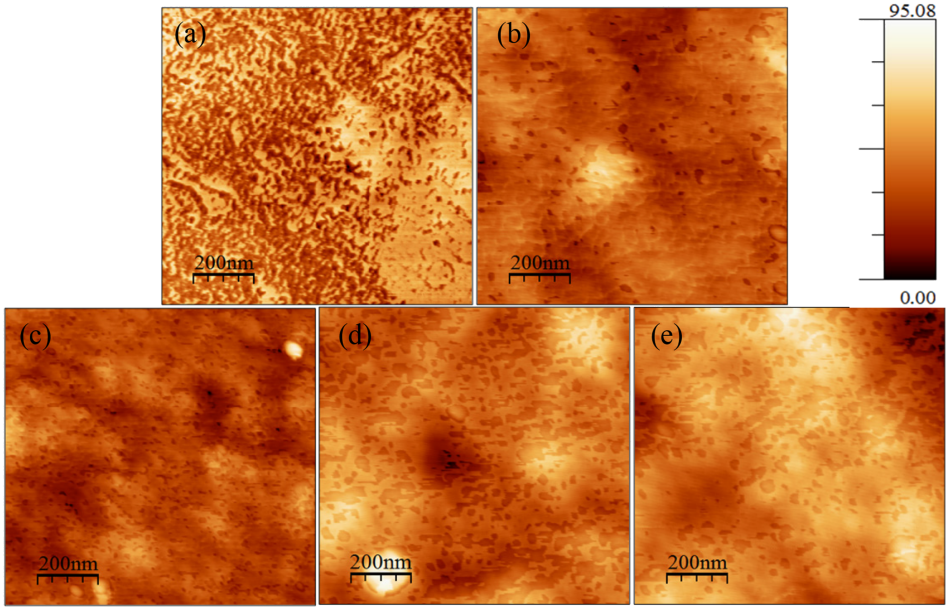

FIG. 2. AFM images of the (a) pristine PEDOT:PSS thin film and (b-e) thin film PEDOT:PSS incorporated with Au NPs at different volume ratios concentrations percentages (0, 2, 4, 6 and 8% respectively).

TABLE I. Summary of tapping mode AFM analysis.

Au NPs solution in PEDOT:PSS %	R_a (nm)	R_{rms} (nm)	Skewness (R_{sk})
0	3.58	4.26	0.084
2	3.37	4.31	0.179
4	3.49	4.41	0.181
6	5.12	6.55	0.207
8	5.46	6.75	0.250

The skewness (R_{sk}) was used to establish the profile symmetry about the mean line. The positive skewness values indicate an asymmetrical height distribution with more peaks than valleys.[21]

The homogenous distribution of the Au NPs in PEDOT:PSS is critical for lateral occurrence of plasmonic effects over the active area of the solar cell. PEDOT:PSS with 4% Au NPs showing better particle distribution and this could have contributed to enhanced plasmonic effect evident by the *J-V* curves. Moreover, the increasing anode surface roughness may result in an increased interface area between the anode and the active layer hence providing shorter transport channels for holes to travel to the ITO. These channels will thus enhance not only hole collection efficiency but also their carrier mobility. This could also have contributed to the high short current density as seen from the *J-V* characteristics. Beyond 4% Au NPs concentration, the surface became too rough.

3. Raman spectroscopy

The Raman spectrum of the pristine and Au NP incorporated PEDOT:PSS of Fig. 3 shows that the most intensive bands appear at 1441 cm^{-1}. This mode is assigned to the symmetric $C_\alpha = C_\beta$ stretching mode of a thiophene ring.[22] Meanwhile, the Raman spectra peaks at 1564 and 1509 cm^{-1} may have originated from two asymmetric $C_\alpha = C_\beta$ stretching vibrations. In addition, the other band peaks at 1369, 1259 and 988 cm^{-1} could be attributed to $C_\beta - C_\beta$ stretching, $C_\alpha - C_\alpha$ inner ring bond, and C – O – C deformation, respectively.[23,24]

Upon incorporation of Au NPs, no shift was observed on the Raman peaks. However, a gradual increase in peak intensities is observed. This could be attributed to a surface enhanced Raman scattering (SERS) effect that is limited by the screening of the PEDOT:PSS.[22] The enhanced local

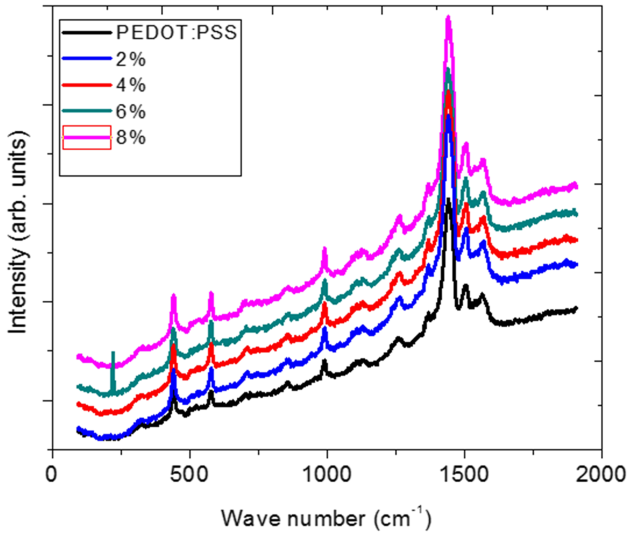

FIG. 3. Raman spectra of pristine PEDOT:PSS and PEDOT:PSS solution with different Au NPs concentrations to illustrate surface enhance Raman scattering in PEDOT:PSS layer.

electromagnetic field resulting from the plasmonically active Au nanoparticles led to an increase in the Raman scattering mode intensity in the PEDOT:PSS hence more light absorption.

B. Optical spectroscopy

1. UV-vis spectroscopy

To elucidate the plasmonic effects due to Au nanoparticles, optical absorption spectra were collected for a solution of PEDOT:PSS with different Au concentrations. In addition, thin films of ITO/PEDOT:PSS+Au/P3HT:PCBM were measured as shown in the UV-vis measurements of Fig. 4. Glass and ITO were taken as the appropriate references for baseline subtraction in order to yield the optical properties of the Au NPs, PEDOT:PSS+Au and PEDOT:PSS+Au/P3HT:PCBM system only. Generally, Au nanospheres display a single peak in the visible range at 510-550 nm wavelength range depending on the shape, size, density and the surrounding nanoparticles media.[25] This is caused by surface plasmon resonance; the presence of a single resonance band (longitudinal mode) in Fig. 4(a) suggests a spherical (symmetric) Au NPs with an aspect ratio of 1. Usually the small sized NPs used in this study, show a dipolar pattern of uniform field in all directions upon absorption as compared to the stronger forward/backward scattering by the big size NPs.[26] The evidence of the surface plasmon resonance effect is presented in the absorption spectra of polymer blend incorporated with Au NPs.

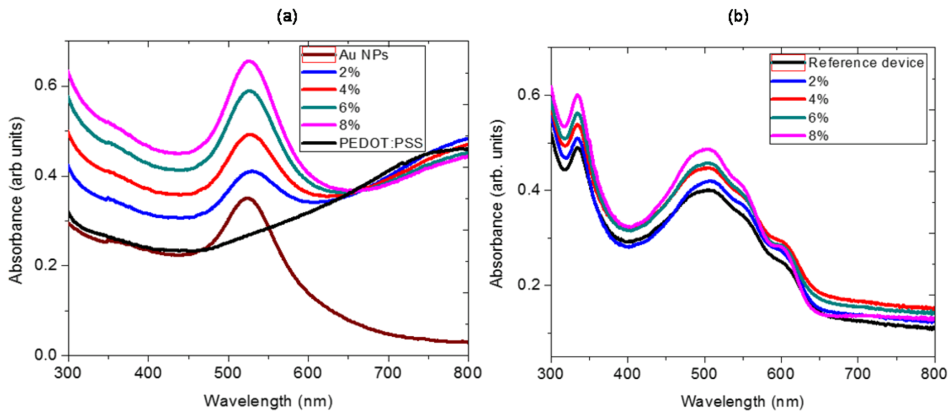

FIG. 4. (a) UV-vis spectra of Au NPs in PEDOT:PSS dispersed at different concentrations and (b) effect of Au NPs in PEDOT:PSS in ITO/PEDOT:PSS+Au/P3HT:PCBM structure.

Indeed the Au NPs have shown large absorption resonances at 525 nm which enhance the π*-π transitions.

The Au surface Plasmon peak developed by the addition of Au nanoparticles to the PEDOT:PSS is evident in Fig. 4(a). The UV-vis measurement showed a marginal absorption enhancement in the active layer (Fig. 4b) which could be attributed to the fact that light incident normal to the ITO produces a very strong near field around the Au NPs attributed to LSPR which is distributed predominantly in the lateral direction along the PEDOT:PSS surface rather than vertically into the adjacent active layer.[20] From Table II, the intensity of the resonance peak upon background subtraction increases with concentration. However, optimum device performance is only realized at 4% Au NPs concentration. This could be attributed to undesirable phenomenon such as dominant parasitic absorption leading to dissipation of maximum heat energy within the nanoparticle without optical excitation of surrounding PEDOT:PSS molecules.[26] The full width at half maximum (FWHM) of Au NPs solution was found to be 142.5 nm. This FWHM reduces upon introducing the NPs solution into PEDOT:PSS to a minimum value of 67.5 nm at 4% concentration and thereafter increases with concentration. This increase could be attributed to the cross-linking of particles into large agglomerates. According to Ghosh *et al.* an effective electromagnetic coupling of clusters is realized for cluster-cluster distances which are smaller than 5 times the cluster radius ($d \leq 5R$, where, d is the center-to-center distance and R is the particle radius) causing coupling of the gold nanoparticle's plasma modes.[27] Moreover, FWHM is also related to the life time of the plasmonic mode hence an increase in broadening with increasing concentration beyond 4% could also be attributed to inter-particle sp's interactions.

C. IV-characterization

Fig. 5 shows direct measurement of the conductance of PEDOT:PSS films with and without Au NPs. As observed in the representative of *J–V* characteristics of the ITO/PEDOT:PSS/Al, the surface resistance of PEDOT:PSS film reduces with incorporation of Au NPs into the PEDOT:PSS layer. This is an indication of an enhanced conductivity of the PEDOT:PSS layer when Au NPs are added.

TABLE II. FWHM and resonance peak intensities for various Au NPs concentration in PEDOT:PSS.

Au NPs solution in PEDOT:PSS %	FWHM (nm)	Peak intensity (a.u.)
Au alone	142.5	0.28
2	84.7	0.10
4	67.5	0.14
6	77.1	0.21
8	86.6	0.26

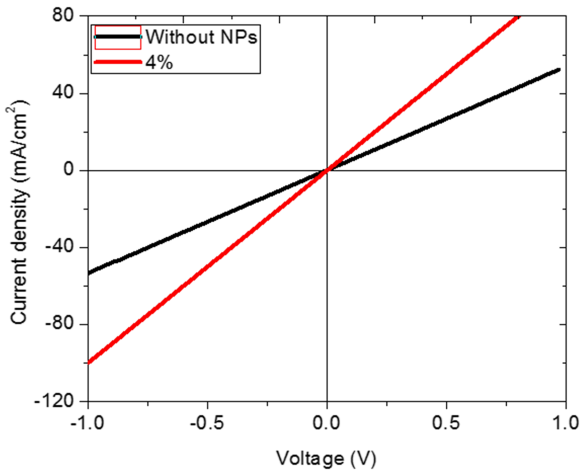

FIG. 5. The *J–V* characteristics representative of pristine ITO/PEDOT:PSS/Al and that with Au NPs incorporated into the hole transport layer (PEDOT:PSS) at 4% concentration.

The use of PEDOT:PSS in organic solar cells usually improves the interface between the active layer and the ITO electrode.[28] According to Girtan *et al* the use of more conductive films of PEDOT:PSS could lead to a free ITO solar cells and consequently to lower cost and longer lifetime full organic solar cells.[29] The Au Nps mixed in the PEDOT:PSS layer are used as hole conductor interface enhancing better extraction of holes after dissociating from the excitons leading to better cell efficiency and even a step towards the realization of an ITO free organic solar cells.

Fig. 6 shows *J–V* characteristics curves of ITO/PEDOT:PSS/P3HT:PCBM/Al solar cells with varied Au NPs concentrations in the PEDOT:PSS and *J–V* characteristic of pristine device without Au NPs for comparison purposes. The devices characteristics and different Au NPs concentrations are listed in Table III. For further investigation of the effect of the Au NPs on device performance when they are incorporated into PEDOT:PSS layer, the *J–V* characteristics of the devices were also measured in the dark as shown in Fig. 6b, and the series resistance (R_s) as well as shunt resistance (R_{sh}) were discussed. The increase in current density could also be attributed to modification of the PEDOT:PSS work function by addition of Au NPs. This is plausible for the 4% AuNPs for which a low intensity of the resonant absorption and high photocurrent are observed.

Fig. 6(a) shows the current density–voltage (*J–V*) characteristics of devices with different Au NPs concentrations in the PEDOT:PSS layer under AM 1.5 G illumination with an intensity of 100 mW cm^{-2}. The detailed OPVs parameters are as outlined in Table III. Fig. 7 shows the hole mobility modelled using the Mott–Gurney law (equation 1) under the assuming negligible deep localized states and field independent mobility:

$$J_{sc} = \frac{9}{8}\mu\varepsilon_0\varepsilon_r\frac{V^2_{in}}{L^3} \tag{1}$$

where μ the charge carrier mobility, ε_0 is the electric permittivity of free space, ε_r the relative dielectric constant of the active layer, V_{in} is the voltage drop across the device and L is the thickness of the device. At optimum device performance (4% Au concentration), the active layer solution recorded an enhanced hole mobility of 12.76×10^{-5} $cm^2V^{-1}s^{-1}$ compared to 10.62×10^{-5} $cm^2V^{-1}s^{-1}$ obtained from a device made without Au NPs.

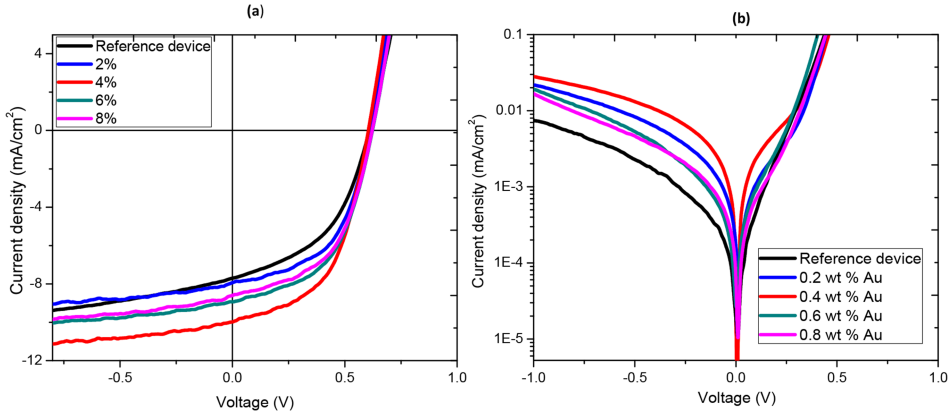

FIG. 6. (a) *J–V* characteristics, recorded under illumination at 100 mW cm^{-2} (AM 1.5G) of devices with incorporated Au nanoparticles in the PEDOT:PSS at different concentrations (b) Semi-log *J–V* characteristics in the dark.

TABLE III. Summary of the performance of the OPVs with varied Au NPs concentration into the PEDOT:PSS.

Au NPs concentration (%)	**J**sc (mA/cm^2)	V_{oc} (V)	FF (%)	PCE (%)	R_s (Ω cm^2)	R_{sh} (Ω cm^2)
0	7.76 ± 0.09	0.60 ± 0.02	52.4 ± 1.0	2.44 ± 0.10	51.6 ± 0.21	237 ± 1
2	7.85 ± 0.12	0.61 ± 0.01	53.1 ± 1.1	2.54 ± 0.08	15.2 ± 0.68	235 ± 2
4	9.94 ± 0.17	0.61 ± 0.01	53.3 ± 1.1	3.23 ± 0.08	10.3 ± 0.68	232 ± 2
6	8.84 ± 0.14	0.61 ± 0.01	53.1 ± 1.4	2.86 ± 0.12	12.5 ± 0.56	264 ± 2
8	8.47 ± 0.13	0.62 ± 0.02	53.0 ± 1.0	2.79 ± 0.01	13.7 ± 0.14	272 ± 4

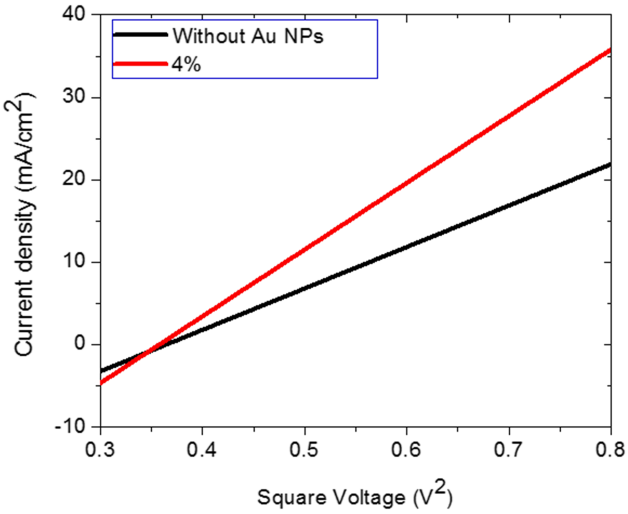

FIG. 7. Linear fit graph of Jsc against V^2 modelled using Mott–Gurney law with an assumption of negligible deep localized states is and field independent mobility.

We predicted that with addition of Au NPs, the Jsc of the devices would increase. It is worth noting that short-circuit current density is affected by various factors such as weak solar spectrum absorbance and poor transport as well as collection of the separated charge carriers at the interface of P3HT and PCBM which were remarkably improved. The Jsc monotonically increased from 7.76 mA/cm^2 for the control device without Au NPs to 7.85 mA/cm^2 with 2% Au to a maximum value of 9.94 mA/cm^2 after adding 4% Au. This could due to the small increase in the spectral absorption as seen in Fig. 4 (b) as well enhanced hole collection capability as indicated by the increased conductivity of the PEDOT:PSS layer through improved and reduced contact resistance. The role of the modification of the PEDOT:PSS work function through AuNPs incorporation can also not be ruled out due to the enhancement of the ohmic behavior of the Au+PEDOT:PSS layers, this assertion is further supported by the hole mobility values determined from SCLC (Mott-Gurney) model. The quality of the device derived from the fill factor improved to a maximum value when 4% Au NPs was used, an indication of improved charge transport. The PCE increased from 2.44% of the control device to 3.23% when the concentration of Au NPs in the PEDOT:PSS was raised to 4%. But, further addition of Au NPs to 6 and 8 wt% led to a lower Jsc of 8.84 and 8.47 mA/cm^2 resulting in a reduction of PCE to 2.86% and 2.79% respectively. Further, Fig. 8 shows the presence of second shunt resistance which indicate that there is a recombination at the electrodes with a minimum degree at 4% Au concentration beyond which the recombination level begin to gradually increase.

However, the Voc of all devices remained almost constant at about 0.61 V. It has been extensively studied that the Voc of PSCs is dependent on the energy difference between the highest occupied molecular orbital (HOMO) level of the donor (P3HT) and the lowest unoccupied molecular orbital (LUMO) level of the receptor (PCBM) when the negative and positive electrodes are in ohmic contact with the P3HT:PCBM used as the active layer.[30] The active materials polymer used and device process in the project are identical prompting the same Voc observed in this project.

Analysis of the series resistances (Rs) and shunt resistances (Rsh) of devices extracted from illuminated *J–V* curves indicate that Rs as well as Rsh first decreases to a minimum value when 4 wt% Au is used. The decrease in Rs is attributed to the reduction of the work function of the PEDOT:PSS by Au NP which reduces the effective device resistance and thus increases the current at the load.

Further investigation of the effect of Au NPs concentration in the PEDOT:PSS layer on the performance of the devices using the *J–V* characteristics of the devices measured in the dark is shown in Fig. 6b. As the Au NPs concentration in PEDOT:PSS increases, the dark current in both the forward and reverse bias first goes up to a maximum value at 4 wt% Au then decreases as the concentration increases. The relatively large leakage current is likely to be due to introduction of

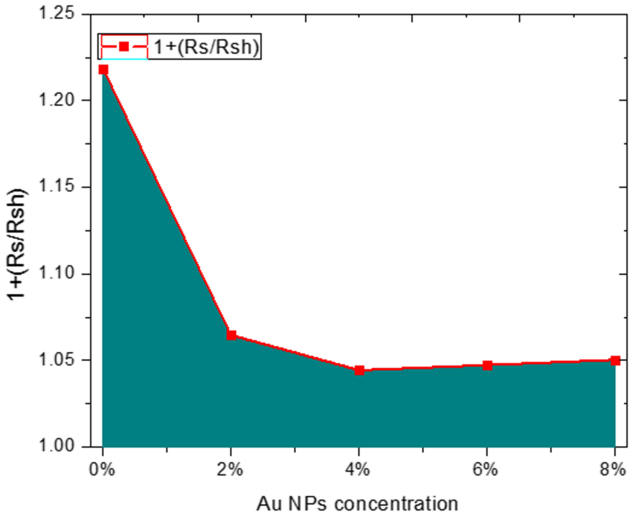

FIG. 8. Plot of 1 + (Rs/Rsh) values versus Rs for different Au NPs concentration.

additional leakage current into the device resulting from increased defects in the hole transport layer that act as recombination centers. At lower concentration the leakage current decreases the shunt resistance. However, as the concentration is increased beyond 4% Au, the improved conductivity of PEDOT:PSS enhances faster travelling of holes to the anode. This leads to reduced excitons quenching and hence less charge recombination since reduction of excitons quenching would compensate the disadvantage of leakage current resulting in an increase in the shunt resistance, R_{sh}. On the other hand creation of interface defect through addition of Au NPs would increase the resistances of the device. However, the presence of Au NPs in the PEDOT:PSS layer leads to reduction of the volume of PEDOT:PSS facilitating movement of the holes towards the anode.[30] This leads to low series resistance with an optimum value giving the highest Jsc observed at 4% Au. This is evident from the conductivity measurement of ITO/PEDOT:PSS/Al device structure shown in Fig. 5 as well as the high hole mobility as observed in Fig. 7. At higher concentration beyond 4% Au, the series resistance increased, reduced contact area between the PEDOT:PSS and the active layer, and PEDOT:PSS morphology changed resulting to undesirable phenomenon such as dominant parasitic absorption leading to dissipation of maximum heat energy within the nanoparticle without optical excitation of surrounding PEDOT:PSS molecules. This could be said to be the cause of low Jsc and PCE beyond 4% Au concentration.

IV. CONCLUSION

In this study, we incorporated Au NPs into the PEDOT:PSS anode buffer layer at various concentrations to improve OSCs performance. The morphological, optical and electrical properties of OSCs with Au NPs have shown enhanced extraction of charge in hole transport layer attributed to the increased injection of charge from Au nanoparticles into PEDOT:PSS layer lowering the resultant energy barrier and promote carrier transport. There was a small increment is visible light absorption with addition of the Au NPs originating from the local surface plasmonic resonance effect of Au NPs. We have demonstrated that for device with Au NPs in PEDOT:PSS the PCE improved by 32.4% mainly originating from J_{sc} and FF. A peak in PCE performance was obtained at an Au NP concentration of 4%.

ACKNOWLEDGMENTS

The authors would like to extend their gratitude to the University of the Witwatersrand, Material Physics Research Institute, School of Physics & Chemistry; and MMU facilities at Wits, NRF and Material Energy Research Group (MERG) for funding. We also wish to acknowledge the additional

support through a bilateral project plasmonics for a better efficiency of solar cells between South Africa and Italy(contributo del Ministero degli Affari Esteri e della Cooperazione Internazionale, Direzione Generale per la Promozione del Sistema Paese).

[1] J. Hou, H.-Y. Chen, S. Zhang, R. I. Chen, Y. Yang, Y. Wu, and G. Li, "Synthesis of a low band gap polymer and its application in highly efficient polymer solar cells," Journal of the American Chemical Society **131**, 15586–15587 (2009).
[2] T. Fleetham, J.-Y. Choi, H. W. Choi, T. Alford, D. S. Jeong, T. S. Lee, W. S. Lee, K.-S. Lee, J. Li, and I. Kim, "Photocurrent enhancements of organic solar cells by altering dewetting of plasmonic Ag nanoparticles," Scientific Reports **5** (2015).
[3] T. D. Nielsen, C. Cruickshank, S. Foged, J. Thorsen, and F. C. Krebs, "Business, market and intellectual property analysis of polymer solar cells," Solar Energy Materials and Solar Cells **94**, 1553–1571 (2010).
[4] Y. Liang, Z. Xu, J. Xia, S. T. Tsai, Y. Wu, G. Li, C. Ray, and L. Yu, "For the bright future—Bulk heterojunction polymer solar cells with power conversion efficiency of 7.4%," Advanced Materials **22** (2010).
[5] M. Jørgensen, K. Norrman, S. A. Gevorgyan, T. Tromholt, B. Andreasen, and F. C. Krebs, "Stability of polymer solar cells," Advanced Materials **24**, 580–612 (2012).
[6] D. E. Motaung, G. F. Malgas, and C. J. Arendse, "Comparative study: The effects of solvent on the morphology, optical and structural features of regioregular poly(3-hexylthiophene): Fullerene thin films," Synthetic Metals **160**, 876–882 (2010).
[7] M. C. Scharber and N. S. Sariciftci, "Efficiency of bulk-heterojunction organic solar cells," Progress in Polymer Science **38**, 1929–1940 (2013).
[8] F. Otieno, M. Airo, K. Ranganathan, and D. Wamwangi, "Annealed silver-islands for enhanced optical absorption in organic solar cell," Thin Solid Films **598**, 177–183 (2016).
[9] C. Sekine, Y. Tsubata, T. Yamada, M. Kitano, and S. Doi, "Recent progress of high performance polymer OLED and OPV materials for organic printed electronics," Science and Technology of Advanced Materials (2016).
[10] I. Kim, D. S. Jeong, T. S. Lee, W. S. Lee, and K.-S. Lee, "Plasmonic nanograting design for inverted polymer solar cells," Optics Express **20**, A729–A739 (2012).
[11] D. Duche, P. Torchio, L. Escoubas, F. Monestier, J.-J. Simon, F. Flory, and G. Mathian, "Improving light absorption in organic solar cells by plasmonic contribution," Solar Energy Materials and Solar Cells **93**, 1377–1382 (2009).
[12] H. Takele, H. Greve, C. Pochstein, V. Zaporojtchenko, and F. Faupel, "Plasmonic properties of Ag nanoclusters in various polymer matrices," Nanotechnology **17**, 3499 (2006).
[13] K. S. Hamdan, S. M. Abdullah, K. Sulaiman, and R. Zakaria, "Effects of silver nanoparticles towards the efficiency of organic solar cells," Applied Physics A **115**, 63–68 (2014).
[14] S.-S. Kim, S.-I. Na, J. Jo, D.-Y. Kim, and Y.-C. Nah, "Plasmon enhanced performance of organic solar cells using electrodeposited Ag nanoparticles," Applied Physics Letters **93**, 305 (2008).
[15] L. Qiao, D. Wang, L. Zuo, Y. Ye, J. Qian, H. Chen, and S. He, "Localized surface plasmon resonance enhanced organic solar cell with gold nanospheres," Applied Energy **88**, 848–852 (2011).
[16] F. X. Xie, W. C. Choy, C. C. Wang, W. E. Sha, and D. D. Fung, "Improving the efficiency of polymer solar cells by incorporating gold nanoparticles into all polymer layers," Applied Physics Letters **99**, 219 (2011).
[17] Y.-S. Hsiao, S. Charan, F.-Y. Wu, F.-C. Chien, C.-W. Chu, P. Chen, and F.-C. Chen, "Improving the light trapping efficiency of plasmonic polymer solar cells through photon management," The Journal of Physical Chemistry C **116**, 20731–20737 (2012).
[18] E. L. Lim, C. C. Yap, M. A. M. Teridi, C. H. Teh, A. R. bin Mohd Yusoff, and M. H. H. Jumali, "A review of recent plasmonic nanoparticles incorporated P3HT: PCBM organic thin film solar cells," Organic Electronics **36**, 12–28 (2016).
[19] F. X. Xie, W. C. Choy, C. C. Wang, E. Wei, and D. D. Fung, "Improving the efficiency of polymer solar cells by incorporating gold nanoparticles into all polymer layers," Applied Physics Letters **99**, 153304 (2011).
[20] D. D. Fung, L. Qiao, W. C. Choy, C. Wang, E. Wei, F. Xie, and S. He, "Optical and electrical properties of efficiency enhanced polymer solar cells with Au nanoparticles in a PEDOT–PSS layer," Journal of Materials Chemistry **21**, 16349–16356 (2011).
[21] S.-Y. Kuo, K.-C. Liu, F.-I. Lai, J.-F. Yang, W.-C. Chen, M.-Y. Hsieh, H.-I. Lin, and W.-T. Lin, "Effects of RF power on the structural, optical and electrical properties of Al-doped zinc oxide films," Microelectronics Reliability **50**, 730–733 (2010).
[22] M. Stavytska-Barba and A. M. Kelley, "Surface-enhanced Raman study of the interaction of PEDOT: PSS with plasmonically active nanoparticles," The Journal of Physical Chemistry C **114**, 6822–6830 (2010).
[23] S. H. Kim, B. M. Park, G. P. Kim, J. Yuh, Y. C. Chang, and H. J. Chang, "Annealing effects of Au nanoparticles embedded PEDOT: PSS in bulk heterojunction organic solar cells," Synthetic Metals **192**, 101–105 (2014).
[24] S. S. Kumar, C. S. Kumar, J. Mathiyarasu, and K. L. Phani, "Stabilized gold nanoparticles by reduction using 3, 4-ethylenedioxythiophene-polystyrenesulfonate in aqueous solutions: Nanocomposite formation, stability, and application in catalysis," Langmuir **23**, 3401–3408 (2007).
[25] A. Tabrizi, F. Ayhan, and H. Ayhan, "Gold nanoparticle synthesis and characterisation," Hacettepe Journal of Biology and Chemistry **37**, 217–226 (2009).
[26] N. Chander, A. Khan, E. Thouti, S. K. Sardana, P. Chandrasekhar, V. Dutta, and V. K. Komarala, "Size and concentration effects of gold nanoparticles on optical and electrical properties of plasmonic dye sensitized solar cells," Solar Energy **109**, 11–23 (2014).
[27] S. K. Ghosh and T. Pal, "Interparticle coupling effect on the surface plasmon resonance of gold nanoparticles: From theory to applications," Chemical Reviews **107**, 4797–4862 (2007).
[28] S.-S. Sun and N. S. Sariciftci, *Organic photovoltaics: mechanisms, materials, and devices* (CRC press, 2005).
[29] M. Girtan and M. Rusu, "Role of ITO and PEDOT: PSS in stability/degradation of polymer: Fullerene bulk heterojunctions solar cells," Solar Energy Materials and Solar Cells **94**, 446–450 (2010).
[30] X. Li, Z. Deng, Y. Yin, L. Zhu, D. Xu, Y. Wang, and F. Teng, "Efficiency enhancement of polymer solar cells with Ag nanoparticles incorporated into PEDOT: PSS layer," Journal of Materials Science: Materials in Electronics **25**, 140–145 (2014).